Journal of ELECTRONIC MATERIALS, Vol. 47, No. 5, 2018
https://doi.org/10.1007/s11664-018-6183-z

A Hydrothermal Route to the Synthesis of $CaTiO_3$ Nanocuboids Using P25 as the Titanium Source

YUXIANG YAN,[1,2] HUA YANG,[1,2,3] XINXIN ZHAO,[2] HAIMIN ZHANG,[2] and JINLONG JIANG[2]

1.—State Key Laboratory of Advanced Processing and Recycling of Non-ferrous Metals, Lanzhou University of Technology, Lanzhou 730050, China. 2.—School of Science, Lanzhou University of Technology, Lanzhou 730050, China. 3.—e-mail: hyang@lut.cn

$CaTiO_3$ nanocuboids (width 0.3–0.5 μm, length 0.8–1.1 μm) have been synthesized by a hydrothermal route using commercial P25 as the titanium source. The as-prepared sample was systematically characterized by means of x-ray powder diffraction, field-emission scanning electron microscopy, field-emission transmission electron microscopy, x-ray photoelectron spectroscopy, Brunauer–Emmett–Teller, ultraviolet–visible diffuse reflectance spectroscopy and electrochemical impedance spectroscopy. The photocatalytic activity of the sample was evaluated by degrading rhodamine B under simulated sunlight irradiation. It is demonstrated that $CaTiO_3$ nanocuboids exhibit superior photocatalytic activity when compared with $CaTiO_3$ nanoparticles. By investigating the effect of scavengers on the dye degradation and the yield of hydroxyl (·OH) radicals, it is concluded that ·OH is the dominant reactive species.

Key words: $CaTiO_3$ nanocuboids, hydrothermal route, P25, photocatalytic activity

INTRODUCTION

Recently, perovskite $CaTiO_3$ has been extensively studied due to its promising ferroelectricity, dielectricity, rare-earth element doping-induced phosphorescence and photocatalytic activity.[1–16] In particular, $CaTiO_3$ has suitable conduction band (CB) and valence band (VB) positions, which are negative and positive to the H^+/H_2 reduction potential and the O_2/H_2O oxidation potential, respectively. Due to this energy band structure, $CaTiO_3$ has been shown to exhibit a pronounced photocatalytic activity for water splitting into hydrogen and oxygen.[7–9] Moreover, $CaTiO_3$ also exhibits a promising capability of photocatalytic degradation of organic pollutants.[10–16]

Semiconductor-based photocatalysis is well known as a heterogeneous surface catalytic reaction, which is highly dependent on the sample morphology, in particular the exposed crystal facets. To address the morphology-mediated tailoring of the photocatalytic performance, various wet-chemistry methods have been widely used to fabricate nanostructures of $CaTiO_3$. Based on those methods, morphologically different $CaTiO_3$ nanostructures like nanoparticles, aggregated prisms, butterfly-like dendrites, nest-like shapes, nanorods, microspheres and nanocuboids have been synthesized.[4–16] In most of the wet-chemistry synthesis routes, titanium complexes (e.g., $Ti(OC_4H_9)_4$, $Ti(OC_3H_7)_4$, $Ti[OCH(CH_3)_2]_4$ and $TiCl_4$) were used as the titanium source. In this work, we report an alternative hydrothermal route to synthesize $CaTiO_3$ nanocuboids using commercial P25 (anatase/rutile mixed-phase TiO_2) as the titanium source. The as-synthesized $CaTiO_3$ nanocuboids exhibit much higher photocatalytic activity toward the degradation of rhodamine B (RhB) than $CaTiO_3$ nanoparticles prepared via a polyacrylamide gel route.

EXPERIMENTAL

Amounts of 0.3329 g (3 mmol) of $CaCl_2$, 0.2396 g (3 mmol) of P25 and 8 g (0.2 mol) of NaOH were

(Received November 28, 2017; accepted February 24, 2018; published online March 8, 2018)

dissolved or dispersed in 20 mL, 20 mL and 40 mL of deionized water, respectively. The P25 suspension and NaOH solution were successively added to the $CaCl_2$ solution drop by drop, during which the mixture was magnetically stirred to make it uniform. The resultant mixture was transformed and sealed into a Teflon-lined stainless steel autoclave with a capacity of 100 mL, followed by heat treatment at 200°C. After 24 h of the hydrothermal reaction, the autoclave was naturally cooled to room temperature. The product was collected by centrifugation, washed several times with deionized water and absolute ethanol, and then dried at 60°C for 12 h. The final $CaTiO_3$ nanocuboids were systematically characterized by x-ray powder diffraction (XRD) with CuKα radiation, field-emission scanning electron microscopy (SEM), field-emission transmission electron microscopy (TEM), N_2 adsorption/desorption technique, x-ray photoelectron spectroscopy (XPS) and ultraviolet–visible diffuse reflectance spectroscopy (UV–Vis DRS).

The flat band potential of $CaTiO_3$ nanocuboids was determined according to the electrochemical impedance spectroscopy (EIS) measurement at different applied potentials in the dark. The EIS measurement was performed on a CST 350 electrochemical workstation using a three-electrode cell configuration consisting of the working electrode, reference electrode (standard calomel electrode; SCE) and counter electrode (platinum foil electrode).[17] The working electrode was prepared by mixing 15 mg of $CaTiO_3$, 0.75 mg of carbon black and 0.75 mg of polyvinylidene fluoride together using 1-methyl-2-pyrrolidione as solvent. The resulting slurry was uniformly spread onto fluorine-doped tin oxide (FTO) glass substrate (1×1 cm^2), and was then dried at 60°C for 5 h. An amount of 0.1 mol L^{-1} (M) Na_2SO_4 aqueous solution was used as the electrolyte.

The photocatalytic activity of the $CaTiO_3$ nanocuboids was evaluated by degrading RhB in aqueous solution (5 mg L^{-1}) under simulated sunlight irradiation from a 200-W xenon lamp. The photocatalyst loading was 0.1 g in 100 mL of RhB solution. During the photocatalysis process, the reaction solution was maintained at room temperature (21°C) by cooling the photocatalytic reactor with a water-cooling system. After 30 min of adsorption in the dark, the mixture was irradiated. The RhB concentration was monitored by measuring the absorbance of the reaction solution at λ = 554 nm on a UV–Vis spectrophotometer. Before measurement, the photocatalyst was removed by centrifugation.

Hydroxyl (·OH) radicals formed over the irradiated photocatalyst were examined by photoluminescence (PL) spectroscopy using terephthalic acid

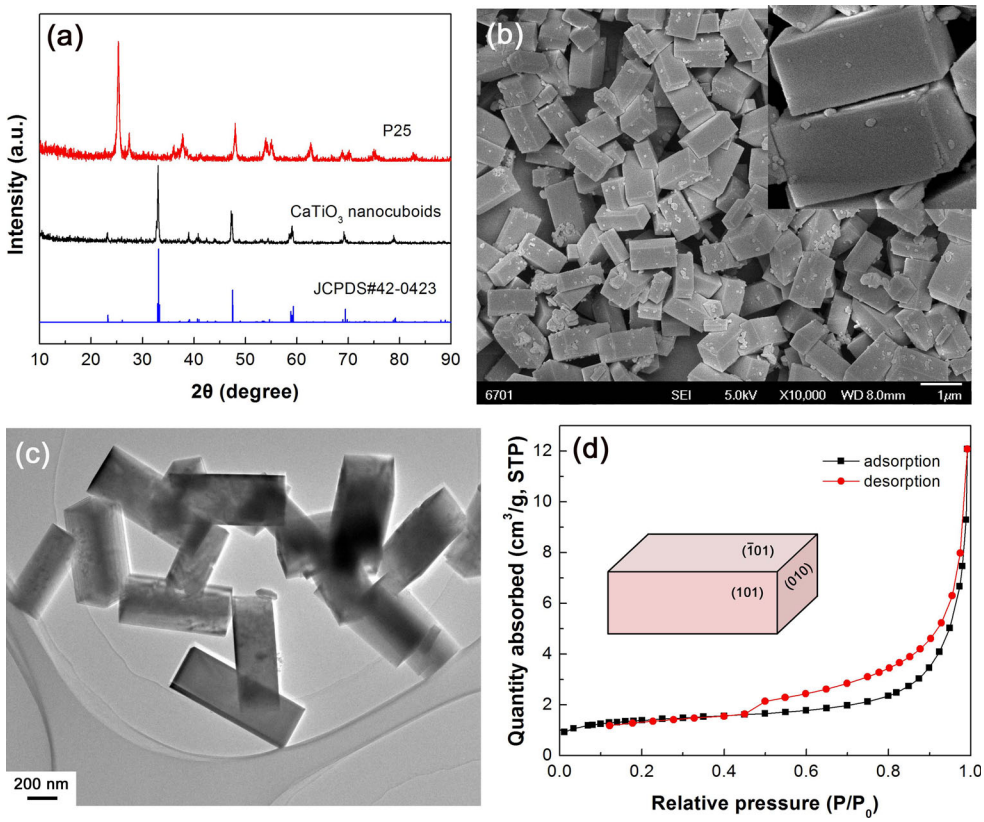

Fig. 1. (a) XRD patterns of $CaTiO_3$ nanocuboids and P25. (b) SEM image of $CaTiO_3$ nanocuboids. Inset the enlarged SEM image of $CaTiO_3$ nanocuboids. (c) TEM image of $CaTiO_3$ nanocuboids. (d) N_2 adsorption–desorption isotherm of $CaTiO_3$ nanocuboids.

(TPA) as a probe for the ·OH radicals. TPA was dissolved in NaOH solution (1.0 mM) to make a 0.25-mM TPA solution. Next, 0.1 g of the photocatalyst was loaded into 100 mL of the TPA solution. The mixture was magnetically stirred in the dark for 30 min, and then irradiated by a 200-W xenon lamp. The PL spectrum of the reaction solution was measured in a fluorescence spectrophotometer with an excitation wavelength of 315 nm.

RESULTS AND DISCUSSION

Figure 1a shows the XRD patterns of the $CaTiO_3$ sample and P25, along with the standard XRD line pattern of $CaTiO_3$ orthorhombic structure (JCPDS#42-0423, a = 5.4424 Å, b = 7.6417 Å, c = 5.3807 Å). It can be seen that the diffraction peaks of the $CaTiO_3$ sample are completely different from those of the precursor P25, and can be perfectly indexed according to the standard diffraction pattern of JCPDS#42-0423. This implies the formation of a single $CaTiO_3$ orthorhombic phase. Figure 1b and c shows the SEM and TEM images of the $CaTiO_3$ sample, respectively. The inset in Fig. 1b shows the enlarged SEM image of the sample. It can be clearly seen that the sample is composed of nanocuboids with the size of 0.3–0.5 μm in width and 0.8–1.1 μm in length. The crystallographic orientation of the nanocuboids, obtained from a previous selected area electron diffraction (SAED) investigation,[9] is schematically shown in the inset in Fig. 1d. Figure 1d shows the N_2 adsorption–desorption isotherm of the sample, which belongs to a type II adsorption isotherm, implying the absence of mesopores in the $CaTiO_3$ nanocuboids. The observation of a small hysteresis loop can be attributed to the existence of surface defects. The Brunauer–Emmett–Teller surface area of the $CaTiO_3$ nanocuboids is found to be 4.88 $m^2\ g^{-1}$.

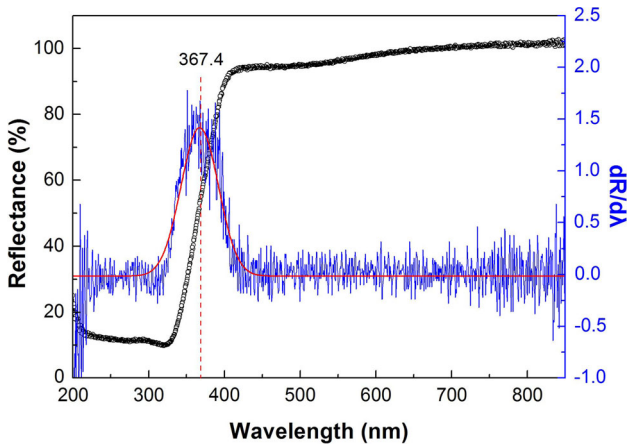

Fig. 3. UV–Vis DRS spectrum of $CaTiO_3$ nanocuboids and its corresponding first-derivative curve.

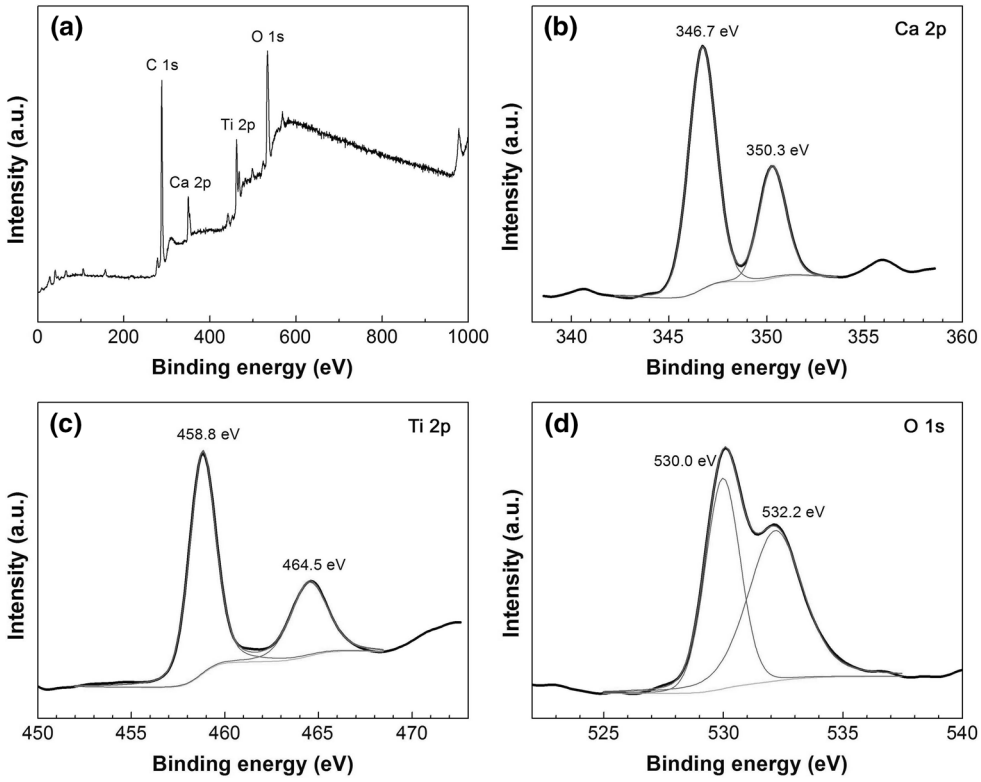

Fig. 2. XPS spectra of $CaTiO_3$ nanocuboids. (a) XPS survey scan spectrum; (b) Ca 2*p* XPS spectrum; (c) Ti 2*p* XPS spectrum; and (d) O 1*s* XPS spectrum.

The chemical states of the elements in the $CaTiO_3$ nanocuboids were investigated by XPS. Figure 2a shows the XPS survey scan spectrum of the sample, clearly revealing the presence of the elements Ca, Ti and O. The adventitious C 1*s* peak at 284.8 eV was used as the XPS binding energy reference. Figure 2b, c, and d shows the high-resolution XPS spectra of Ca 2*p*, Ti 2*p* and O 1*s*, respectively. The Ca 2*p* XPS spectrum presents two sharp peaks at 346.7 eV (Ca $2p_{3/2}$) and 350.3 eV (Ca $2p_{1/2}$), while the Ti 2*p* XPS spectrum shows two peaks at 458.8 eV (Ti $2p_{3/2}$) and 464.5 eV (Ti $2p_{1/2}$). No additional peaks are visible. This implies that Ca and Ti are in the form of Ca(II) and Ti(IV) oxidation states, respectively.[18,19] The O 1*s* XPS signal is deconvoluted into two peaks at 530.0 eV and 532.2 eV, which are ascribed to the crystal lattice oxygen and the surface adsorbed oxygen, respectively.[20]

Figure 3 shows the UV–Vis DRS spectrum of the $CaTiO_3$ nanocuboids and the corresponding first-derivative curve of the spectrum. From the peak on

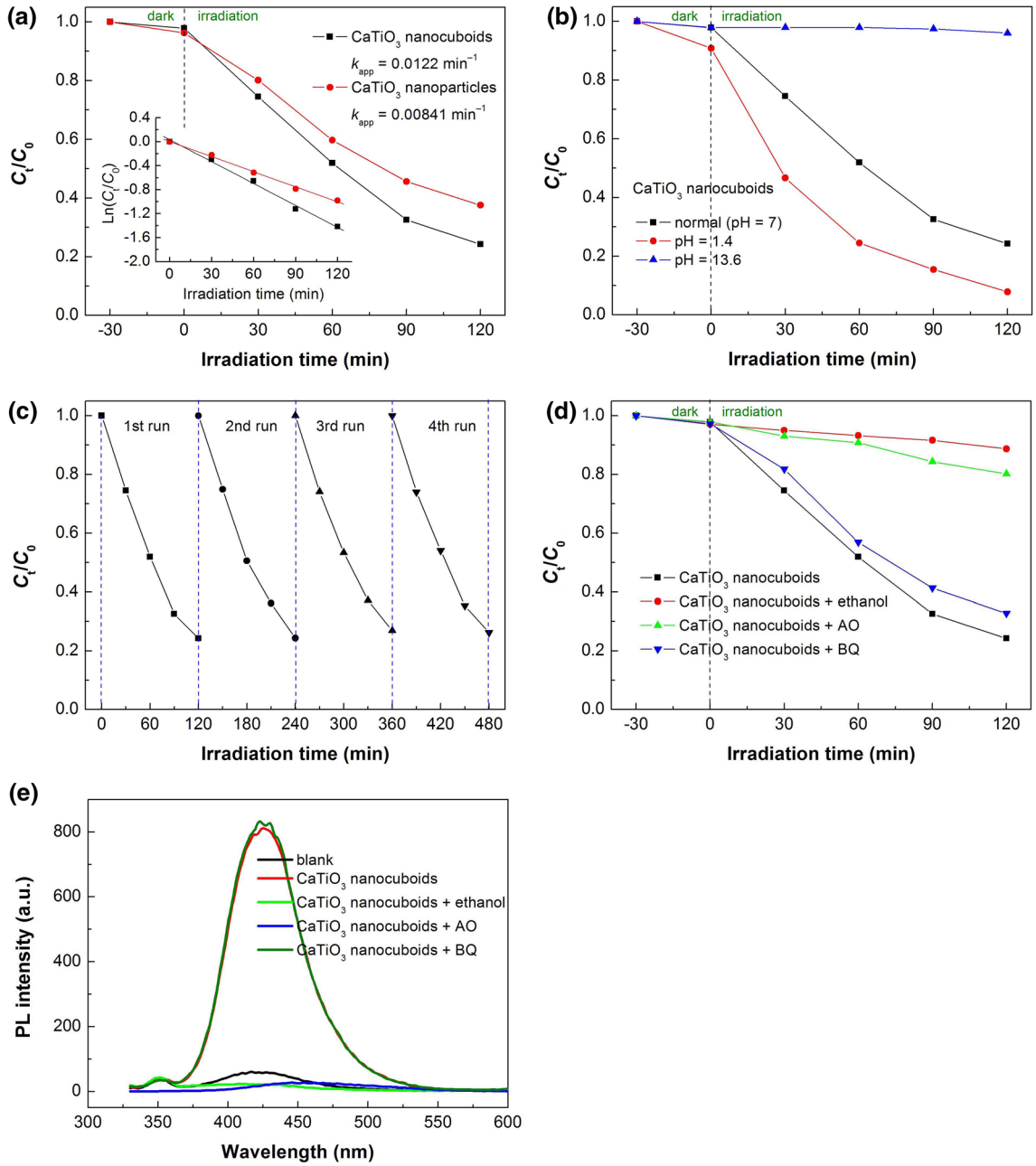

Fig. 4. (a) Comparison of the photocatalytic activity between $CaTiO_3$ nanocuboids and nanoparticles for the RhB degradation. (b) Effect of pH on the RhB degradation over $CaTiO_3$ nanocuboids. (c) Photocatalytic stability of $CaTiO_3$ nanocuboids toward the RhB degradation on reusing four times. (d) Effect of ethanol, AO, and BQ on the RhB degradation over $CaTiO_3$ nanocuboids. (e) Effect of ethanol, AO, and BQ on the PL spectrum of the TPA solution over $CaTiO_3$ nanocuboids.

the first-derivative curve, the absorption edge of the $CaTiO_3$ nanocuboids is obtained as 367.4 nm, implying that they have a bandgap energy of 3.38 eV.

We compared the photocatalytic activity of $CaTiO_3$ nanocuboids with that of $CaTiO_3$ nanoparticles prepared via a polyacrylamide gel route ($\sim$ 55 nm)[13] by degrading RhB under simulated sunlight irradiation. Figure 4a shows the the time-dependent photocatalytic degradation of RhB over $CaTiO_3$ nanocuboids and nanoparticles. The degradation percentage of RhB is given as $(C_0 - C_t)/C_0 \times 100\%$ (C_0 = initial RhB concentration, C_t = the remaining RhB concentration). After 120 min of photocatalysis, the degradation percentage of the dye reaches 76% for the $CaTiO_3$ nanocuboids and 62% for the $CaTiO_3$ nanoparticles. The apparent first-order reaction rate constant (k_{app}), derived from the plots of $Ln(C_t/C_0)$ versus t (as shown by the inset in Fig. 4a), demonstrates that the former has a photocatalytic activity 1.5 times higher than the latter. It is noted that the photocatalytic activity of a semiconductor depends greatly on its morphology and size, and generally small particle size favors good photocatalytic activity.[21] In this work, the $CaTiO_3$ nanoparticles used for the photocatalytic comparison have an average size of 55 nm, which is much smaller than the size of the $CaTiO_3$ nanocuboids. However, a relatively higher photocatalytic activity is observed for the $CaTiO_3$ nanocuboids. This could be ascribed to the fact that $CaTiO_3$ nanocuboids have specially exposed (010) and (101) facets. The RhB degradation in the acidic and alkaline environments (adjusted by the addition of HNO_3 or NaOH) over the $CaTiO_3$ nanocuboids were also investigated. As shown in Fig. 4b, the dye degradation is significantly enhanced at pH 1.4, but completely inhibited at pH 13.6. A possible reason is that $CaTiO_3$ could have a much higher surface energy in the acidic environment than in the alkaline environment. In addition, $CaTiO_3$ nanocuboids are found to exhibit an excellent photocatalytic stability. As shown in Fig. 4c, the degradation percentage of RhB after irradiation for 120 min still reaches a high value of 74% in the 4th cycle of the photocatalysis, and only 2% loss of the dye degradation is observed as compared to the dye degradation in the 1st cycle of the photocatalysis.

To reveal the reactive species, ethanol, benzoquinone (BQ) and ammonium oxalate (AO) were used as the scavengers of ·OH, superoxide ($\cdot O_2^-$) and hole (h^+), respectively,[22] to investigate their effect on the dye degradation. As shown in Fig. 4d, the addition of ethanol (5 mL) or AO (1 mM) to the reaction solution has a significant suppression on the dye degradation, whereas only a minor suppression of the dye degradation is observed on the addition of BQ (1 mM). This implies that the dye degradation is highly correlated with ·OH and h^+. Figure 4e shows the effect of ethanol, BQ and AO on the PL spectra of the TPA solution (reaction for 120 min). In the absence of scavengers or with the addition of BQ, the TPA solution shows an obvious PL signal at $\sim$ 429 nm, implying the production of ·OH radicals. However, the ·OH radicals are quenched by ethanol or AO, since no obvious PL signal is observed with their addition. On the basis of the above information, it is concluded that ·OH is the dominant reactive species in the present photocatalytic system, and derives mainly from the reaction of photogenerated h^+ with OH^-/H_2O.

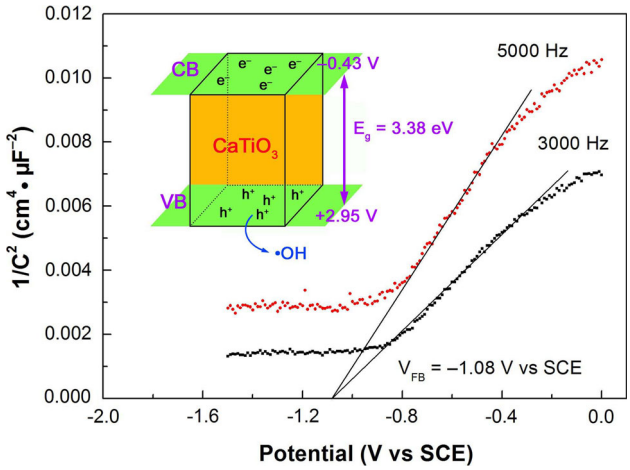

Fig. 5. Mott–Schottky plots of $CaTiO_3$ nanocuboids obtained at different frequencies. Inset potential energy diagram for $CaTiO_3$ nanocuboids.

The flat band potential V_{FB}, which is roughly equal to the conduction band potential of an n-type semiconductor, can be determined using the Mott–Schottky equation.[23,24] Figure 5 shows the Mott–Schottky plots obtained at different frequencies for the $CaTiO_3$ nanocuboids, from which the V_{FB} is obtained by extrapolating the linear portion of the plots to the V axis. The potential versus SCE reference electrode can be converted to the potential versus normal hydrogen electrode (NHE) according to $V(NHE) = V(SCE) + 0.059pH + 0.242$ (here pH = 7).[25] The CB and VB potentials of $CaTiO_3$ are therefore obtained as – 0.43 and + 2.95 V versus NHE, respectively, as shown by the inset in Fig. 5. It is obvious that the VB potential of $CaTiO_3$ is positive to the redox potentials of $H_2O/\cdot OH$ (+ 2.38 V vs. NHE) and $OH^-/\cdot OH$ (+ 1.99 V vs. NHE), implying that the photogenerated h^+ can thermodynamically react with OH^-/H_2O to produce ·OH.

CONCLUSIONS

Based on a hydrothermal route, $CaTiO_3$ nanocuboids with the size of 0.3–0.5 μm in width and 0.8–1.1 μm in length were synthesized using commercial P25 as the titanium source. The photocatalytic experiment demonstrates that $CaTiO_3$ nanocuboids exhibit a photocatalytic activity higher than $CaTiO_3$ nanoparticles toward RhB degradation. The CB and VB potentials of $CaTiO_3$ nanocuboids measured by EIS measurement are – 0.43 and + 2.95 V versus

NHE, respectively, ·OH is determined to be the dominant reactive species in the present photocatalytic system.

ACKNOWLEDGEMENT

This work was supported by the National Natural Science Foundation of China (Grant No. 51662027).

REFERENCES

1. M.D. Biegalski, L. Qiao, Y.J. Gu, A. Mehta, Q. He, Y. Takamura, A. Borisevich, and L.Q. Chen, *Appl. Phys. Lett.* 106, 162904 (2015).
2. J. Sedlacek, P. Ctibor, J. Kotlan, and Z. Pala, *Surf. Eng.* 29, 384 (2013).
3. A. Maddu, L. Permatasari, and A. Arif, *J. Ceram. Process. Res.* 18, 146 (2017).
4. S.C. Pereira, A.T. Figueiredo, C.M. Barrado, M.H. Stoppa, Y. Dwivedi, M.S. Li, and E. Longo, *J. Braz. Chem. Soc.* 26, 2339 (2015).
5. X. Chen, Y. Li, F. Kong, L. Li, Q. Sun, and F. Wang, *J. Alloy. Compd.* 541, 505 (2012).
6. J. Zhuang, Q. Tian, S. Lin, W. Yang, L. Chen, and P. Liu, *Appl. Catal. B Environ.* 156–157, 108 (2014).
7. T. Alammara, I. Hamma, M. Warkb, and A.V. Mudring, *Appl. Catal. B Environ.* 178, 20 (2015).
8. S.N. Lim, S.A. Song, Y.C. Jeong, H.W. Kang, S.B. Park, and K.Y. Kim, *J. Electron. Mater.* 46, 6096 (2017).
9. T. Kimijima, K. Kanie, M. Nakaya, and A. Muramatsu, *CrystEngComm* 16, 5591 (2014).
10. W. Dong, B. Song, G. Zhao, W. Meng, and G. Han, *Appl. Phys. A* 123, 348 (2017).
11. L.M. Lozano-Sáncheza, S. Obregón, L.A. Díaz-Torres, S.W. Lee, and V. Rodríguez-González, *J. Mol. Catal. A Chem.* 410, 19 (2015).
12. W. Dong, Q. Bao, X. Gu, and G. Zhao, *J. Ceram. Soc. Jpn.* 123, 643 (2015).
13. Y.S. Huo, H. Yang, T. Xian, J.L. Jiang, Z.Q. Wei, R.S. Li, and W.J. Feng, *J. Sol–Gel. Sci. Technol.* 71, 254 (2014).
14. M. Ye, M. Wang, D. Zheng, N. Zhang, C. Lin, and Z. Lin, *Nanoscale* 6, 3576 (2014).
15. X. Yan, X. Huang, Y. Fang, Y. Min, Z. Wu, W. Li, J. Yuan, and L. Tan, *Int. J. Electrochem. Sci.* 9, 5155 (2014).
16. H. Zhao, Y. Duan, and X. Sun, *New J. Chem.* 37, 986 (2013).
17. Z.M. Cui, H. Yang, and X.X. Zhao, *Mater. Sci. Eng. B* 229, 160 (2018).
18. S.K. Park, T.K. Yun, and J.Y. Bae, *J. Nanosci. Nanotechnol.* 16, 2571 (2016).
19. C. Han, J. Liu, W. Yang, Q. Wu, H. Yang, and X. Xue, *J. Sol–Gel. Sci. Technol.* 81, 806 (2017).
20. L.J. Di, H. Yang, T. Xian, and X.J. Chen, *Materials* 10, 1118 (2017).
21. F. Wang, H. Yang, H.M. Zhang, and J.L. Jiang, *J. Mater. Sci. Mater. El.* 29, 1304 (2018).
22. X. Zhao, H. Yang, Z. Cui, R. Li, and W. Feng, *Mater. Technol.* 32, 870 (2017).
23. F. Cardon and W.P. Gomes, *J. Phys. D Appl. Phys.* 11, L63 (1978).
24. A. Fattah-alhosseini, *Arab. J. Chem.* 9, S1342 (2016).
25. F. Wang, H. Yang, and Y.C. Zhang, *Mat. Sci. Semicon. Proc.* 73, 58 (2018).